Sand moisture assessment using instantaneous phase information in ground penetrating radar data

Yu Zhang, Dylan Burns, Dryver Huston, Tian Xia

School of Engineering, University of Vermont, 33 Colchester Ave, Burlington, VT 05405, USA

ABSTRACT

In this paper, a method using the instantaneous phase information of the reflection ground penetrating radar (GPR) signal to detect the variation of sand moisture is developed. The moisture changes the permittivity of the medium, which results in different speed when the GPR electromagnetic (EM) wave propagates in the medium. In accordance to this principle, we develop an analytical method to extract GPR reflection signal's instantaneous phase parameters utilizing Hilbert Transform for sand moisture characterization. For test evaluation, Finite Difference Time Domain (FDTD) numerical simulations using a 3rd party open source program GprMax V2.0, and laboratory experiments on sand samples are conducted using a commercial GPR (2.3 GHz Mala CX) as the data acquisition system.

Keywords: Ground penetrating radar, instantaneous phase, Hilbert transform, sand moisture content, dielectric constant, FDTD simulation

1. INTRODUCTION

Saturated sand region in road subsurface layer is a sign of the early stage of roadway sinkhole formation, railroad ballast contamination and sub-base degradation. Non-destructive test of the subsurface saturated region can prevent safety hazards and costly emergency repair on roadway and railway. GPR is a major subsurface imaging tool for non-destructive infrastructure inspection [1].

To characterize the subsurface moisture content, the approach of GPR backscattering signal amplitude measurement has been extensively utilized [2-5]. For EM wave transmitting through the subsurface medium of different moisture levels, the signal attenuation factor is different. Hence, the backscattering amplitude implies different levels of moisture. However, to derive accurate quantitative relationship between the backscattering signal amplitude and the medium moisture (through dielectric property characterization) is very complicated.

As shown in Figure 1, the GPR signal is emitted from the transmitter antenna into the subsurface medium and the receive antenna collects the backscattering signals. For the study in this paper, the top layer is the sand layer with various moisture contents and the base layer is the dry concrete. A_1 is the echo from the air-sand interface, A_2 is the echo from the interface between the sand layer and the concrete layer, and A_3 is the echo from the bottom of the concrete layer. The echo signal A_2 is measured to monitor the moisture variations in the sand layer. To accurately measure A_2 amplitude is not trivial, as it can be easily contaminated by noise, interference and other surface layer reflection signals.

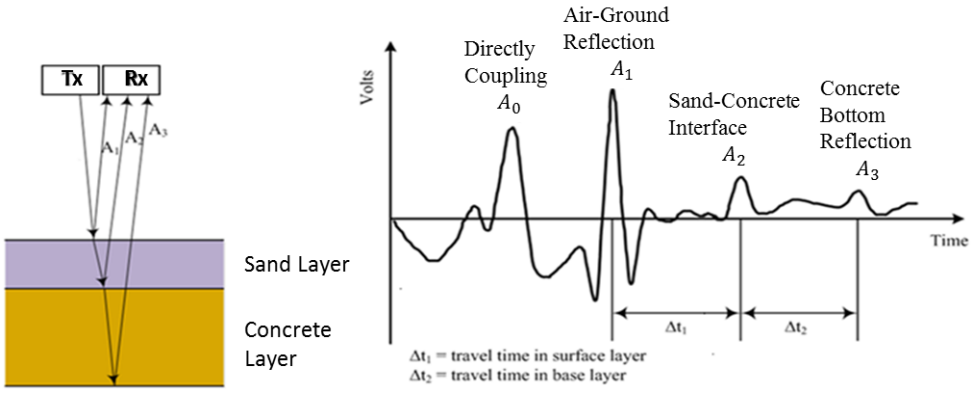

Figure 1 GPR detection scheme

To overcome such obstacle, in this paper, we investigate measuring the moisture through the characterization of the instantaneous phase parameters of GPR reflection signal. Microwave laboratory measurements in [8] revealed the presence of persistent and coherent phase variations in a temporal sequence of DInSAR (differential interferometric synthetic aperture radar) images, where the correlation between radar signal phase variation and soil moisture was investigated. The study sheds light on utilizing EM signal phase information to measure soil moisture. As soil moisture changes, the dielectric constant of the medium also changes, which results in different EM wave propagation speed in the medium. Thus, when an EM wave transmits through subsurface sand layers of different moisture levels, its phase delay will be altered. In this study, Hilbert Transform is explored to extract GPR signal phase parameter. An EM wave transmission model is also developed to approximately interpret the quantitative relationship between phase behavior and medium moisture content.

The remaining sections of this paper are organized as follows. In Section 2, the Hilbert Transform is utilized to characterize GPR signal phase information, and EM wave phase variation model is developed. In section 3, FDTD (Finite Difference Time Domain) numerical simulations using GprMax V2.0 are performed to analyze GPR reflection signal phase variations in mediums of different moisture content. In section 4, laboratory moisture measurement experiments are conducted, where a ground coupled 2.3 GHz Mala CX is used as the data acquisition system. Section 5 contains the concluding remarks.

2. METHODOLOGY

2.1 Instantaneous phase extraction

Hilbert Transform (HT) finds its widely utilization in communication system receiver design for baseband signal extraction. In our GPR moisture detection scheme, Hilbert Transform is implemented to extract the pulse signal envelope and the instantaneous phase parameter.

The Hilbert Transform of signal $s(t)$ can be considered as the convolution of $s(t)$ with the function $h(t) = \frac{1}{\pi t}$, which can be expressed as

$$\hat{s}(t) = \mathcal{H}\{s\} = h(t) * s(t) = \int_{-\infty}^{\infty} s(\tau)h(t-\tau)d\tau = \frac{1}{\pi}\int_{-\infty}^{\infty} \frac{s(\tau)}{t-\tau} d\tau \quad (1)$$

To avoid the singularities when $\tau = t$ and$\tau = \pm\infty$, Hilbert Transform is defined using the Cauchy principal value. thus,

$$\hat{s}(t) = \mathcal{H}\{s\} = -\frac{1}{\pi}\lim_{\varepsilon \downarrow 0} \int_{\varepsilon}^{\infty} \frac{s(t+\tau)-s(t-\tau)}{\tau} d\tau \quad (2)$$

Applying HT to GPR signal $s(t)$, the analytic signal is obtained as

$$s_a(t) = s(t) + i\hat{s}(t) \quad (3)$$

where $\hat{s}(t)$ is the direct output of the Hilbert Transform of $s(t)$. The magnitude of $s_a(t)$ equals

$$|s_a(t)| = \sqrt{s(t)^2 + \hat{s}(t)^2} \quad (4)$$

$|s_a(t)|$ is the envelope of $s(t)$, which can be used for signal power characterization.

The instantaneous phase of $s_a(t)$ equals

$$\varphi_a(t) = arg\{s_a(t)\} = \tan^{-1}(\frac{\hat{s}(t)}{s(t)}) \quad (5)$$

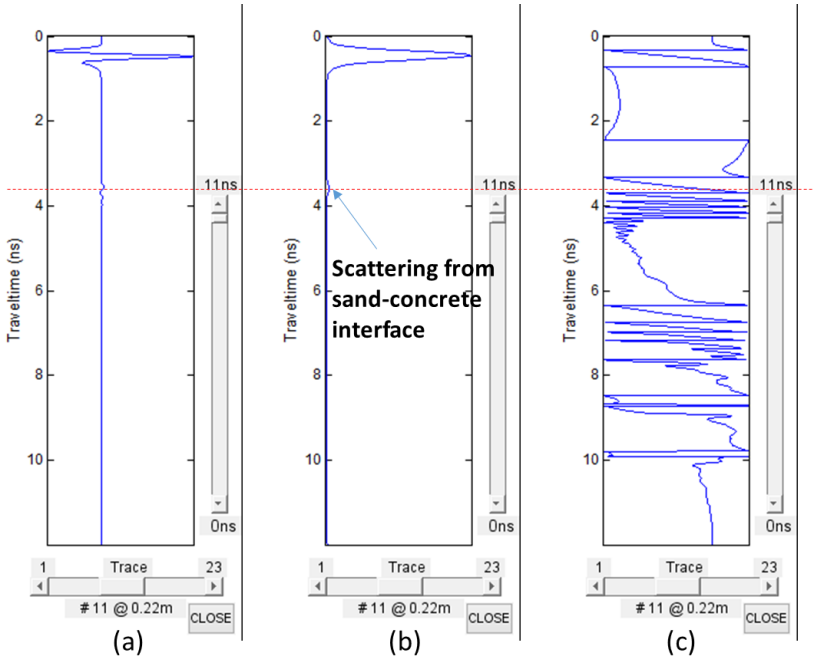

Figure 2 Instantaneous phase measurement using Hilbert Transform: (a) GPR A-Scan waveform; (b) Signal envelope; (c) Instantaneous phase.

In our GPR detection scheme, the amplitude envelope is first computed to detect the peak of echo from the sand-concrete interface. The instantaneous phase value at the same time point is then recorded. As an example, Figure 2(a) depicts a GPR A-Scan signal waveform, Figure 2(b) and 2(c) plot the signal envelope and instantaneous phase obtained upon Hilbert Transform respectively. In the envelop waveform, the first peak at 0.50 ns represents the air-sand interface echo, and the second peak at 3.75 ns is the sand-concrete interface echo.

2.2 Phase behavior model

In this section, analytic model is presented to describe the phase changes of the signal in relation to the sand dielectric properties.

Considering the sand layer as a lossy medium with complex dielectric constant $\varepsilon = \varepsilon_r - j\varepsilon_i$, the propagation of the signal through a distance z into the medium can be modeled by

$$S(z) = S_0 e^{-\gamma z} = S_0 e^{-(\alpha+j\beta)z} = S_0 e^{-\alpha z} e^{-j\beta z} \tag{6}$$

where the propagation constant γ is [9]

$$\gamma = \alpha + j\beta = j\frac{2\pi}{\lambda}\sqrt{\varepsilon_r - j\varepsilon_i} = jk\sqrt{\varepsilon_r - j\varepsilon_i} \tag{7}$$

where λ is the wavelength, and $k = 2\pi/\lambda$ is the wavenumber. The first exponential term in (6) specifies the propagation signal amplitude attenuation through the medium, whereas the second term specifies the propagation phase change. To solve the α and β, following transformation of Eq. (7) is performed:

$$\gamma^2 = (\alpha + j\beta)^2 = (\alpha^2 - \beta^2) + j2\alpha\beta \tag{8}$$

$$\gamma^2 = (jk\sqrt{\varepsilon_r - j\varepsilon_i})^2 = -k^2(\varepsilon_r - j\varepsilon_i) = -k^2\varepsilon_r + jk^2\varepsilon_i \tag{9}$$

Comparing the real parts and imaginary parts of Eq. (8) and (9) respectively, following equations can be obtained:

$$\begin{cases} \alpha^2 - \beta^2 = -k^2\varepsilon_r \\ 2\alpha\beta = k^2\varepsilon_i \end{cases} \tag{10}$$

Solving Eq. (10), the signal amplitude attenuation parameter α and phase delay parameter β can be expressed as

$$\alpha = k\sqrt{|\varepsilon|}\sin\frac{\theta}{2} \tag{11}$$

$$\beta = k\sqrt{|\varepsilon|}\cos\frac{\theta}{2} \tag{12}$$

where $\tan\theta = \varepsilon_i/\varepsilon_r$. Eq. (12) indicates that the instantaneous propagation phase change is determined by the loss tangent angle θ and the dielectric constant ε. In our GPR measurement, the thickness of the medium under test is assumed uniform. In other words, for measurements at different locations, the reflection signal phase variation from the sand-concrete interface is solely dependent on the variation of dielectric constant of the sand.

Behavior model of ε in [10] for a sandy soil shows the complex dielectric constant is dominated by the real part, which allows the approximation $\varepsilon \cong \varepsilon_r$. Thus, the tangent angle θ is very small and $\cos\frac{\theta}{2}$ equals approximately 1. Eq. (12) can be approximated as

$$\beta = k\sqrt{|\varepsilon|}\cos\frac{\theta}{2} \cong k\sqrt{|\varepsilon|} \cong k\sqrt{|\varepsilon_r|} \tag{13}$$

The phase change for a two-way path is obtained by [9]

$$\Delta\phi = 2kd(\sqrt{|\varepsilon_m|} - \sqrt{|\varepsilon_n|}) \tag{14}$$

where d is the vertical thickness of wet sand layer, and the subscripts represent the dielectric constant values at different measurements m and n.

According to Eq. (14), an approximately linear relationship exists between change of instantaneous phase and square root of the magnitude of the medium dielectric constant. In next section, the relationship between medium dielectric constant and moisture content is elaborated, and the instantaneous phase behavior is correlated with the medium moisture content.

2.3 Dielectric constant vs. moisture content

Dielectric constant measurements on five different soil types at frequencies between 1.4 and 18 GHz have been perform in [10], which found that soil texture has a pronounced effect on dielectric behavior, especially at frequencies below 5 GHz. Based on these measurements, separate polynomial expressions relating the real and imaginary part of ε to the volumetric moisture content m_v, and the percentage of sand and clay are derived in [11]. These polynomial expressions are of the form

$$\varepsilon_r = (a_0 + a_1S + a_2C) + (b_0 + b_1S + b_2C)m_v + (c_0 + c_1S + c_2C)m_v^2 \tag{15}$$

$$\varepsilon_i = (d_0 + d_1S + d_2C) + (e_0 + e_1S + e_2C)m_v + (f_0 + f_1S + f_2C)m_v^2 \tag{16}$$

where S is the percentage (by weight) of sand, C is the percentage (by weight) of clay, and a_i, b_i, c_i, d_i, e_i, f_i are frequency dependent coefficients. Knowing the EM wave penetrating depth, numerical values for these coefficients at different frequencies can be evaluated [8]. Eq. (15) and (16) can be used to estimate the dielectric constant of the sand at the given observation frequency should the weight coefficients be known.

According to the results in [10] ~ [12], m_v^2 is the dominant term in Eq. (15). Thus, approximation can be made as $\varepsilon_r \sim O(m_v^2)$. Considering $\Delta\phi$ is linearly proportional to $\Delta\sqrt{|\varepsilon|}$ as Eq. (14) shows, $\Delta\phi$ is about linearly proportional to the moisture content variation Δm_v. Therefore, once the instantaneous phase variation in GPR signal is detected, the moisture content in medium can be estimated.

3. FDTD SIMULATIONS

In this section, FDTD simulations on a mock-up sand-concrete structure with various dielectric constants of sand layer are performed to verify the instantaneous phase behavior upon medium dielectric constant.

3.1 FDTD scheme

For validation purposes, GPR signal phase behavior simulations with a mock-up geometry structure shown in Figure 3 are performed. The structural geometry emulates a concrete base covered with a sand layer. The top air layer is 5 cm thick, the sand layer is 15 cm thick and the concrete layer is 30 cm thick. A UWB GPR signal is generated to scan the

structure and the instantaneous phase of the echo from sand-concrete interface is extracted for analysis purpose. Dielectric parameter values for air, sand and concrete layers are listed in Table 1 referring [13]. To emulate the sand dielectric property changes due to moisture content variations, 14 groups of simulations with sand dielectric constants varying from 8 to 20 are performed.

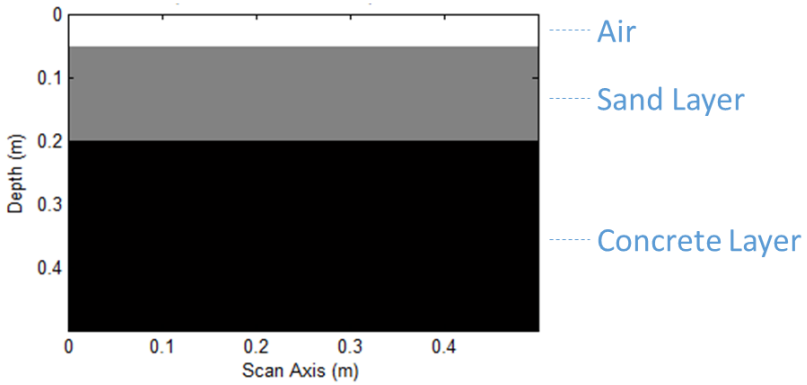

Figure 3 Geometry model for FDTD simulations

Table 1 Typical values of relative permitivity and conductivity for geological materials

Material	ε_r	σ_e (mS/m)
Air	1	0
Dry Sand	4	0.01
Saturated Sand	20	0.1
Concrete	6	0.01

The FDTD method is employed to develop the computational model characterizing GPR signal propagation in the geometry structure. FDTD is a grid-based differential numerical modeling method that discretized Maxwell's equations using central-difference approximations to both the space and time partial derivatives. In this study, the transverse electric (TE) mode is adopted, and perfectly matched layer (PML) absorbing boundaries model is applied to eliminate reflections from the edges of the modeling grid. The governing TE mode field equation are [14]:

$$\frac{\partial E_x}{\partial t} = \frac{1}{\varepsilon}\left(\frac{\delta H_z}{\delta y} - \sigma E_x\right) \tag{17}$$

$$\frac{\partial E_y}{\partial t} = \frac{1}{\varepsilon}\left(\frac{\delta H_z}{\delta x} - \sigma E_y\right) \tag{18}$$

$$\frac{\partial H_z}{\partial t} = \frac{1}{\mu}\left(\frac{\delta E_x}{\delta y} + \frac{\delta E_y}{\delta x} - \frac{\delta \mu}{\varepsilon} H_z\right) \tag{19}$$

where E_x and E_y are transverse electrical field components, and H_z is the longitudinal magnetic field component. ε, σ, and μ specify medium's permittivity, conductivity and permeability respectively.

To compute the electrical field and the magnetic field, Yee scheme [15] is applied to discretize, both in time and space, the above TE mode governing equations with central difference approximations. In our simulations, the GPR test signal is generated as 2.3 GHz central frequency Ricker (first derivative of the Gaussian) waveform. In order to achieve fine resolution and accuracy, we set the FDTD spatial increment Δx as 2.5 mm, which produces 50 samples per wavelength at high end of the excitation spectrum. While the temporal step is computed correspondingly as $\Delta t = \frac{\Delta x}{c\sqrt{2}} = 5.9\,ps$ to ensure the stability condition (c is the light speed in air. The FDTD simulation tool is GprMax V2.0 program [16].

3.2 Simulation results

In each simulation, the sand-concrete interface echo is first identified using the signal envelope with the Hilbert Transform. The corresponding instantaneous phase value is extracted. According to the explanation in Sec. 2, the phase difference $\Delta\phi$ is linearly proportional to$\Delta\sqrt{|\varepsilon|}$. Using the measurement with $\varepsilon = 8$ as the reference, the $\Delta\phi$ vs $\Delta\sqrt{|\varepsilon|}$ for all other measurements are normalized and plotted in Figure 4.

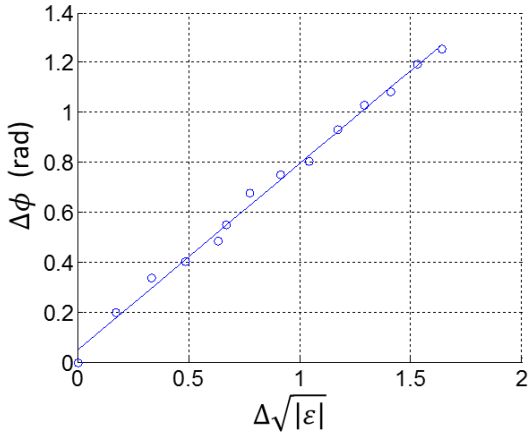

Figure 4 Simulated variation in phase from the sand-concrete interface

In Figure 4, the circular dots are the measured $\Delta\phi$ at various $\Delta\sqrt{|\varepsilon|}$, and the straight line approximates the linear regression curve, which shows that the instantaneous phase variation slope is about 0.7090 rad per unit $\Delta\sqrt{|\varepsilon|}$, which is in good agreement with the calculation result 0.6283 rad per unit $\Delta\sqrt{|\varepsilon|}$ using Eq. (14). Thus, the numerical simulation result is consistent with the quantitative phase behavior model in Sec. 2. Furthermore, considering the moisture sand thickness is 15 cm, the measured instantaneous phase variation rate can be normalized as $0.7090 \div 15 = 0.0473$ rad per unit $\Delta\sqrt{|\varepsilon|}$ for sand with 1 cm thickness.

4. LABORATORY EXPERIMENTS

The approximately linear relationship between the instantaneous phase and medium moisture content is validated through laboratory experiments on sand box setup with sand moisture level varying from 30% (dry) – 100% (saturated).

4.1 Test configuration

As shown in Figure 5, the GPR test is configured with a sand bag buried in a sand box, whose dimension is 85 cm long, 40 cm wide and 11.5 cm deep. The thickness of the buried sand bag is 3 cm. The sand box is put on the dry concrete floor. For each test, 50 mL water is added into the sand bag, and the corresponding moisture content of the sand in bag is then measured using Lincoln 24-Inch Soil Moisture Meter #8002 [17]. A ground coupled 2.3 GHz Mala CX GPR system [18] is used as data acquisition system. In total, six sets of GPR data are collected with the sand moisture content varying from 30% to 100%.

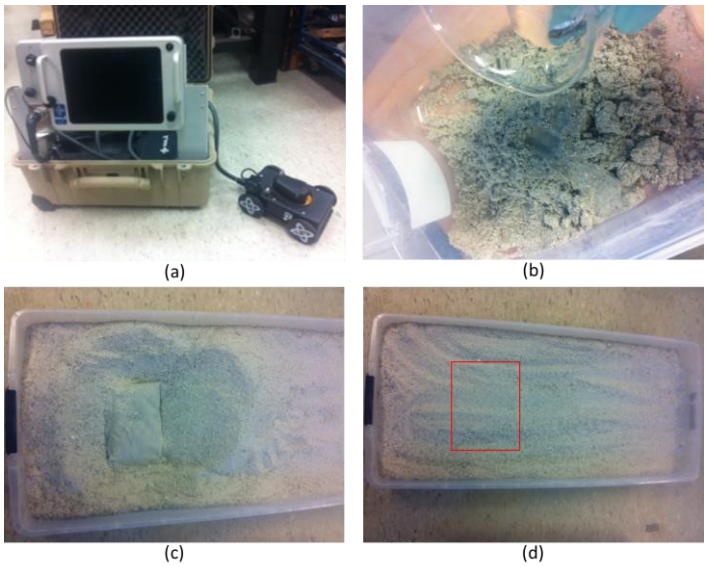

Figure 5 Lab sand box experiments: (a) 2.3 GHz Mala CX GPR system; (b) Sand mixed with 50 mL water each time; (c) Moisten sand buried in a box containing dry sand; (d) Sand box test scene.

In the experiments, the sand dielectric constants with different moisture contents are also measured. The dielectric constant of sand is deduced by measuring the EM wave propagation time in sand [19]. For a medium with a dielectric constant ε, the speed of waves propagating in this medium is

$$V = C/\sqrt{\varepsilon} \tag{20}$$

where $C = 2.998 \times 10^8\ m/s$. And the round-trip traveling time is

$$t = 2d/V \tag{21}$$

where d is the thickness of sand layer. Thus, the dielectric constant ε can be obtained as

$$\varepsilon = (C \cdot \frac{t}{2d})^2 \tag{22}$$

The measured dielectric constants of sand under various moisture contents are shown in Table 2.

Table 2 Dielectric constant of sand under various moisture content

Moisture Content	Dielectric Constant of Sand
30%	8.148
40%	9.342
55%	10.792
70%	12.869
80%	14.488
100%	16.553

4.2 Experimental results

For processing the measured GPR signal, the sand-concrete interface echo is first identified through the signal envelope extraction using Hilbert Transform. Then the corresponding instantaneous phase value is then recorded. According to analysis in Sec. 2, the phase difference $\Delta\phi$ between each measurement is linear proportional to the moisture

content variation Δm_v. Using the measurement for sand moisture level $m_v = 30\%$ as the reference, the $\Delta\phi$ vs Δm_v relationship for all other five measurements are normalized and plotted in Figure 6(a).

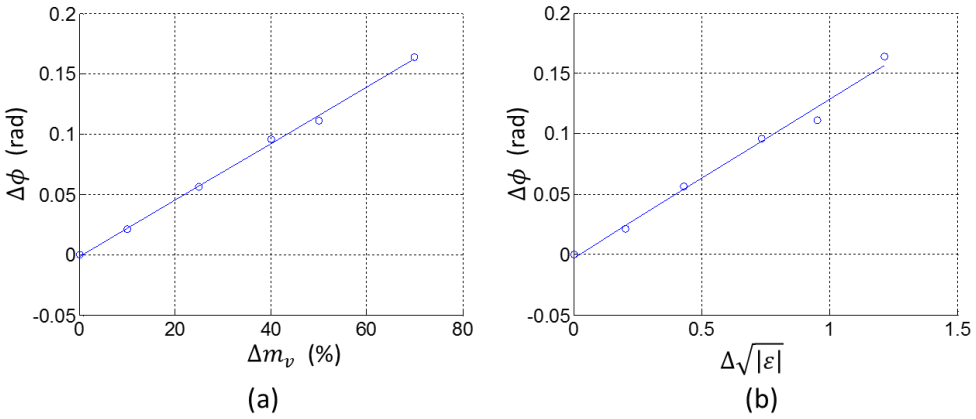

Figure 6 Variation in phase from the sand-concrete interface in lab sand box experiments: (a) Relationship between $\Delta\phi$ and Δm_v; (b) Relationship between $\Delta\phi$ and $\Delta\sqrt{|\varepsilon|}$.

In Figure 6(a), the circle dots are the measured $\Delta\phi$ and the straight line is the linear regression curve approximating the relationship between $\Delta\phi$ and Δm_v. The changing rate of the instantaneous phase according to the regression curve in Figure 6 is 0.0023 rad per 1% moisture content variation.

Figure 6(b) plots the $\Delta\phi$ and $\Delta\sqrt{|\varepsilon|}$ for all the six groups of measurements after normalization. The circular dots are the measured $\Delta\phi$ at various $\Delta\sqrt{|\varepsilon|}$, and the straight line approximates the linear regression curve. The regression curve slope is 0.1313 rad per unit $\Delta\sqrt{|\varepsilon|}$. Since the thickness of the sand bag is 3 cm, the normalized instantaneous phase variation rate is calculated as $0.1313 \div 3 = 0.0437$ rad per unit $\Delta\sqrt{|\varepsilon|}$ for sand with 1 cm thickness. Comparing to the simulation result in Sec. 3 that phase variation rate is 0.0473 rad per unit $\Delta\sqrt{|\varepsilon|}$ for sand with 1 cm thickness, the measurement error is $\frac{(0.0473-0.0437)}{0.0473} \times 100\% = 7.61\%$.

5. CONCLUSIONS

This paper develops the method using the instantaneous phase parameter of GPR reflection signal to measure sand moisture. A linear approximation between the instantaneous phase ϕ and the square root of medium dielectric constant $\sqrt{|\varepsilon|}$ is derived through quantitative modeling, and is validated through FDTD simulations. The presence of approximately linear relationship between instantaneous phase difference $\Delta\phi$ and medium moisture content change Δm_v are also demonstrated in lab experiments. In the future, we will refine the study and explore its application for monitoring medium moisture in other structures, such as asphalt pavement and railroad ballast.

REFERENCE

[1] Jol, H.M., [Ground penetrating radar theory and applications], Elsevier (2008).

[2] Al-Qadi, I.L., Xie, W., Roberts, R. and Leng, Z., "Data Analysis Techniques for GPR used for Assessing Railroad Ballast in High Radio-Frequency Environment," Journal of Transportation Engineering, ASCE 136(4), 392–399 (2010).

[3] Zhang, Y., Venkatachalam, A.S., Xie, Y., Wang, G. and Xia, T., "Data Analysis Techniques to Leverage Ground Penetrating Radar Ballast Inspection Performance," 2014 IEEE Radar Conference, Cincinnati, OH, May 19-23 (2014).

[4] Xia, T., Xu, X., Venkatachalam, A. and Huston, D., "Development of a High Speed UWB GPR for Rebar Detection," Proceedings of IEEE International Conference on Ground Penetrating Radar (GPR) (2012).

[5] Venkatachalam, A., Xu, X., Huston, D. and Xia, T., "Development of a New High Speed Dual Channel Impulse Ground Penetrating Radar," IEEE Journal of Selected Topics in Applied Earth Observations and Remote Sensing 7(3), 753–760 (2014).
[6] Huston, D., [Structural sensing, health monitoring, and performance evaluation], CRC Press, 117 (2010).
[7] Zhang, Y., Venkatachalam, A.S., Huston, D. and Xia, T., "Advanced signal processing method for ground penetrating radar feature detection and enhancement," Proc. SPIE 9063, Nondestructive Characterization for Composite Materials, Aerospace Engineering, Civil Infrastructure, and Homeland Security 2014, 906318 (2014).
[8] Morrison, K., Bennett, J.C., Nolan, M. and Menon, R., "Laboratory Measurement of the DInSAR Response to Spatiotemporal Variations in Soil Moisture," IEEE Transactions on Geoscience and Remote Sensing 49(10), 3815-3823 (2011).
[9] Morrison, K., Bennett, J.C. and Nolan, M., "Using DInSAR to Separate Surface and Subsurface Features," IEEE Transactions on Geoscience and Remote Sensing 51(6), 3424-3430 (2013).
[10] Hallikainen, M.T., Ulaby, F.T., Dobson, M.C. and El-Rayes, M.A., "Microwave dielectric behavior of wet soil – Part 1: Empirical models and experimental observations," IEEE Transactions on Geoscience and Remote Sensing GE-23(1), 25-34 (1985).
[11] Dobson, M.C., Ulaby, F.T., Hallikainen, M.T. and El-Rayes, M.A., "Microwave Dielectric Behavior of Wet Soil – Part II: Dielectric Mixing Models," IEEE Transactions on Geoscience and Remote Sensing GE-23(1), 35-46 (1985).
[12] Behari, J., [Microwave Dielectric Behavior of Wet Soils], Remote Sensing and Digital Image Processing 8, Springer (2005).
[13] Giannopoulos, A., "The investigation of Transmission-Line Matrix and Finite-Difference Time-Domain Methods for the Forward Problem of Ground Probing Radar," D.Phil thesis, Department of Electronics, University of York, UK (1997).
[14] Sadiku, M., [Numerical Techniques in Electromagnetics with Matlab], CRC Press (2009).
[15] Yee, K.S., "Numerical Solution of Initial Boundary Value Problems Involving Maxwell's Equations in Isotropic Media," IEEE Transactions on Antennas and Propagation 14, 302-307 (1966).
[16] Giannopoulos, A., "Modelling ground penetrating radar by GprMax," Construction and Building Materials 19(10), 755-762 (2005).
[17] Lincoln 24-Inch Soil Moisture Meter #8002: http://frostproof.com/lincoln-24-inch-soil-moisture-meter-8002/
[18] Mala CX System: http://www.malags.com/products/mala-cx-%28concrete-imaging%29-system
[19] Xu, X., Xia, T., Venkatachalam, A. and Huston, D., "The Development of A High Speed Ultrawideband Ground Penetrating Radar for Rebar Detection," ASCE Journal of Engineering Mechanics 139(3), 272-285 (2013).